Amphiphilic block copolymers in oil-water-surfactant mixtures: efficiency boosting, structure, phase behaviour and mechanism



2001 J. Phys.: Condens. Matter 13 9055

(http://iopscience.iop.org/0953-8984/13/41/302)

INSTITUTE OF PHYSICS PUBLISHING JOURNAL OF PHYSICS: CONDENSED MATTER

J. Phys.: Condens. Matter **13** (2001) 9055–9074 PII: S0953-8984(01)24861-9

# Amphiphilic block copolymers in oil–water–surfactant mixtures: efficiency boosting, structure, phase behaviour and mechanism

**G Gompper**[1], **D Richter**[1] **and R Strey**[2]

[1] Institut für Festkörperforschung, Forschungszentrum Jülich, 52425 Jülich, Germany
[2] Institut für Physikalische Chemie, Universität zu Köln, Luxemburger Strasse 116, 50939 Köln, Germany

Received 16 May 2001, in final form 18 May 2001
Published 28 September 2001
Online at stacks.iop.org/JPhysCM/13/9055

**Abstract**

The effect of amphiphilic block copolymers on the phase behaviour and structure of ternary microemulsions in water, oil and non-ionic surfactant mixtures is reviewed. Recent experiments have revealed that the addition of small amounts of polyethylenepropylene–polyethyleneoxide block copolymer to the ternary systems leads to a dramatic increase in the volumes of oil and water solubilized into a bicontinuous microemulsion for a given surfactant volume fraction. While phase diagrams directly show the power of the amphiphilic block copolymers as efficiency boosters, the theoretical analysis in terms of bending energy discloses the mechanism for the efficiency boosting as due to the variation of the surfactant film curvature elasticity by tethered polymers in the form of mushrooms at the interface. Neutron scattering experiments employing a high-precision two-dimensional contrast variation technique confirm this picture and demonstrate that the polymer molecules uniformly decorate the surfactant film.

## 1. Introduction

In microemulsions—thermodynamically stable and macroscopically homogeneous mixtures of water, oil and surfactant—the surfactant molecules form an extended interfacial film separating water and oil on a local scale. Recently, we discovered an enormous efficiency increase of the emulsification capacity of the non-ionic surfactant by adding amphiphilic block copolymers of polyethylenepropylene–polyethyleneoxide (PEP–PEO) type. While mixtures of two surfactants of similar chain length show only small synergistic effects in microemulsions, adding the amphiphilic block copolymer to a conventional microemulsion system was found to lead to an efficiency boosting, as we called it, for even very small concentrations of polymer (Jakobs *et al* 1999).

0953-8984/01/419055+20$30.00  

The theoretical understanding of microemulsions has progressed by use of statistical physical models. The Ginzburg–Landau models, which describe ternary mixtures by the local density fields of all the components, are particularly useful, as are the interfacial (or membrane) models, which describe the physics of the amphiphile film by its curvature elasticity. A recent overview by Gompper and Schick (1994b) reviews the state of the art.

The structural properties of such complex fluids may be accessed by small-angle neutron scattering (SANS), which takes advantage of the unique possibility to vary the contrast between the different components by hydrogen–deuterium exchange. A number of systematic studies on the bicontinuous microemulsions under either oil–water or film contrast have been reported in the literature. Pieruschka and Safran have calculated the scattering intensities under bulk (Pieruschka and Safran 1993) and film (Pieruschka and Safran 1995) contrast within the curvature elasticity approach. Ginzburg–Landau-type theories with a single scalar order parameter—the local concentration difference between oil and water—reveal the structure factor for ternary microemulsions under bulk-contrast conditions. The so-called Teubner–Strey formula (Teubner and Strey 1987) is employed routinely in order to describe such scattering results. The scattering under film contrast has been studied by Roux *et al* (1990, 1992) as well as Gompper and Schick (1994a). In this case, Ginzburg–Landau models with two scalar order parameters are required in order to describe the thermal fluctuations of the amphiphile concentration in microemulsions, which in turn was shown to be strongly influenced by the oil–water correlation function.

In this paper, we review the analysis of a coherent set of scattering results on bicontinuous microemulsions with varying polymer concentrations. We evaluate the different partial structure factors and interpret the results for the bulk and film contrasts jointly in terms of both the Ginzburg–Landau and interfacial models (Endo *et al* 2000, 2001). The analysis of the film scattering is facilitated by an analytic theoretical expression, which was obtained recently for the curvature model. We study the effect of the polymers on the various parameters of the theory and evaluate the system parameters on the basis of the structural information. Furthermore, the polymer scattering itself is studied by extracting the polymer–polymer partial structure factor. This quantity provides information about the polymer conformation and polymer density in the system. In particular, we show that all polymer chains are tethered to the surfactant films. Detailed information on the density profile of the tethered chains can be obtained from the interference term between the polymer and film scattering.

Theoretically, the polymer decoration of surfactant films is expected to affect both the bending rigidity and the saddle splay modulus. According to our present understanding, the phase diagrams of microemulsions are determined by the elastic moduli, the bending modulus and the saddle-splay or Gaussian-curvature modulus of the surfactant film. Recently, Morse (1994) and Golubović (1994) as well as Gompper and Kroll (1998) demonstrated an exponential dependence of the phase boundary of the homogeneous phase in terms of the surfactant volume fraction on the magnitude of the saddle-splay modulus. Polymers tethered to a surfactant layer modify the elasticity moduli and thus are expected to have a profound effect on the phase diagrams. As it turns out, the efficiency boosting effect of the tethered polymers is explained in terms of the variation of the saddle-splay modulus by the tethered chains (Endo *et al* 2000).

## 2. Theory

### *2.1. Curvature model of membrane ensembles*

The structure and phase behaviour of ternary amphiphilic mixtures has been intensively studied theoretically since the mid-eighties of the last century. Microscopic lattice models,

Ginzburg–Landau models and interfacial models have all been employed in these investigations (Gompper and Schick 1994b). Each class of model has its own merits. For the description of microemulsion and sponge phases in highly dilute systems, i.e. in systems where the amphiphile concentration is very low, interfacial models seem to be both most appropriate and most predictive. In these models, the surfactant sheets are modelled by a mathematical surface, the shapes and fluctuations of which are controlled by the curvature elastic energy (Canham 1970, Helfrich 1973)

$$\mathcal{H} = \int \mathrm{d}S\,[2\kappa(H - c_0)^2 + \bar{\kappa}K] \tag{1}$$

where $H$ and $K$ are the mean and Gaussian curvature, respectively, which can be expressed as

$$H = \tfrac{1}{2}(c_1 + c_2) \qquad K = c_1 c_2 \tag{2}$$

in terms of the principal curvatures $c_1$ and $c_2$ at each point of the surface. In this model, the phase behaviour depends on five parameters, which are the bending moduli $\kappa$ and $\bar{\kappa}$, the spontaneous curvature $c_0$, the surfactant volume fraction $\psi$, and the ratio, $\phi_o/\phi_w$, of oil and water volume fractions.

While this model looks deceptively simple, it presents a very difficult problem of statistical physics. Therefore, only the results of rather crude analytical approximations (Safran *et al* 1986, Andelman *et al* 1987, Cates *et al* 1988, Golubović and Lubensky 1989, 1990, Porte *et al* 1989, Porte 1992, Safran 1992, Pieruschka and Marčelja 1992, Pieruschka and Safran 1993, 1995, Morse 1994, Golubović 1994, Wennerström and Olsson 1993, Daicic *et al* 1995a, b, c, Morse 1997, Tlusty *et al* 1997, 2000) and computer simulations (Pieruschka and Marčelja 1994, Gompper and Kroll 1998, 2000) are available so far. Therefore, no unanimous agreement about the form of the free energy, not even for balanced systems with $c_0 = 0$, has been reached so far. Most authors agree that the membrane fluctuations on small length scales lead to a renormalization of the elastic moduli on a length scale $\ell$, which is given by (Peliti and Leibler 1985, Helfrich 1985, David 1989)

$$\kappa_R(\ell) = \kappa - \frac{\alpha}{4\pi} k_B T \ln(\ell/\delta_0) \tag{3}$$

$$\bar{\kappa}_R(\ell) = \bar{\kappa} + \frac{\bar{\alpha}}{4\pi} k_B T \ln(\ell/\delta_0) \tag{4}$$

where $\delta_0$ is the size of the surfactant molecules. The values of the (universal) prefactors of the logarithms in (3) and (4) are also under debate. Field-theoretic calculations (Peliti and Leibler 1985, David 1989, Cai *et al* 1994) for almost planar membranes give

$$\alpha = 3 \qquad \bar{\alpha} = 10/3. \tag{5}$$

They imply a softening of the membrane at larger scales. However, the values $\alpha = -1$ and $\bar{\alpha} = 0$ have also been suggested recently (Helfrich 1998).

In microemulsions and sponge phases, the logarithmic renormalization is cut off at length scales which correspond to the average domain size of the oil or water regions. This happens at $\ell \sim \psi^{-1}$. Therefore, microemulsions should coexist with almost pure oil and water phases when $\bar{\kappa}_R(\psi^{-1}) = 0$ (Morse 1994), or

$$\ln(\psi) = \frac{4\pi}{\bar{\alpha}} \frac{\bar{\kappa}}{k_B T}. \tag{6}$$

This picture was questioned a few years ago by Daicic *et al* (1995a, b, c), who explicitly denied the existence of a logarithmic renormalization in bicontinuous microemulsions. Previous experimental evidence (Porte *et al* 1991) seems indeed not completely conclusive,

since the composition of the membrane along the investigated dilution path had not been controlled (Porte *et al* 1997).

However, the renormalization picture described above is now strongly supported by recent computer simulations (Gompper and Kroll 1996, 1998), which show excellent agreement with (6).

### 2.2. *Membranes decorated by amphiphilic block copolymers*

The effect of polymers attached to membranes on their curvature elasticity has been calculated recently (Hiergeist and Lipowsky 1996, Eisenriegler *et al* 1996, Marques and Fournier 1996) for Gaussian (ideal) chains. In the mushroom regime, where there is little or no interaction between neighbouring polymers on the membrane, the effective curvature moduli are found to be

$$\kappa_{eff} = \kappa_0 + \frac{k_B T}{12}\left(1 + \frac{\pi}{2}\right)\sigma(R_o^2 + R_w^2) \tag{7}$$

$$\bar{\kappa}_{eff} = \bar{\kappa}_0 - \frac{k_B T}{6}\sigma(R_o^2 + R_w^2) \tag{8}$$

$$c_{0,eff}(T) = c_0(T) + \frac{1}{4}\sqrt{\frac{\pi}{6}}\frac{k_B T}{\kappa_{eff}}\sigma(R_w - R_o) \tag{9}$$

where $\kappa_0$, $\bar{\kappa}_0$ and $c_0(T)$ are the bending rigidity, saddle-splay modulus and spontaneous curvature of the pure surfactant membrane, respectively, and $\sigma$ is the number density of polymer anchoring points on the membrane. Obviously, for a symmetric block copolymer, with $R_w = R_o$, the spontaneous curvature contribution of the polymer vanishes. However, (9) shows that the fish-tail point with $T = \tilde{T}$, where the mean curvature vanishes, can also be reached for asymmetric block copolymers, since the spontaneous curvature of the surfactant film and that induced by the polymer may cancel, so that

$$c_0(\tilde{T}) = -\frac{1}{4}\sqrt{\frac{\pi}{6}}\frac{k_B \tilde{T}}{\kappa_{eff}}\sigma(R_w - R_o) \tag{10}$$

at this point. The experimental results for the temperature dependence of the spontaneous curvature of the pure surfactant film can therefore be used to determine the effect of the block copolymer on the membrane curvature. Equation (9) also explains why the shape of the fish tail remains essentially unchanged with increasing polymer concentration, but shifts in temperature. The reason is that the polymer contribution is nearly temperature independent, so that there is just a constant offset between $c_{0,eff}(T)$ and $c_0(T)$.

The results for the dependence of the membrane volume fraction $\psi$ on the saddle-splay modulus, equation (6), and for the dependence of the saddle-splay modulus on the polymer grafting density, equation (8), can now be combined to predict the dependence of the fish-tail point on the polymer grafting density $\sigma$ and the polymer size. A simple superposition approach gives immediately (Endo *et al* 2000)

$$\ln(\psi) = \ln(\psi^{(0)}) - \Xi\sigma(R_w^2 + R_o^2) \tag{11}$$

where $\psi^{(0)}$ is the surfactant volume fraction of the fish-tail point in a system without polymer, and

$$\Xi = \frac{2\pi}{3\bar{\alpha}} = \frac{\pi}{5} = 0.628\ldots \tag{12}$$

for Gaussian (ideal) chains and $\bar{\alpha} = 10/3$.

### 2.3. Bulk and film scattering

Berk (1987, 1991), Teubner (1991), Pieruschka and Marčelja (1992) and Pieruschka and Safran (1993, 1995) have suggested that the interfaces be modelled in microemulsions as level surfaces of Gaussian random fields. This approach is most useful and predictive when the Gaussian model of random interfaces is related to the statistical mechanics of microemulsions by a variational approximation (Pieruschka and Safran 1993, 1995). The starting point is a Gaussian free-energy functional of the general form

$$\mathcal{H}_0[\phi] = \int \mathrm{d}^3q\, \nu(\boldsymbol{q})^{-1}\phi(\boldsymbol{q})\phi(-\boldsymbol{q}). \tag{13}$$

The spectral density $\nu(\boldsymbol{q})$ in the functional (13) is determined by the requirement that the $\phi(\boldsymbol{r}) = 0$ level surfaces mimic the behaviour of interfaces controlled by the curvature Hamiltonian (1) as well as possible. With such a variational approach, Pieruschka and Safran (1993) were able to relate the parameters in the bulk scattering intensity to the curvature elastic moduli $\kappa$ and $\bar{\kappa}$.

The film correlation function, $g_{ff}(r)$, can also be calculated for the Gaussian-random-field model. It was found to be approximated very well for large $r$ by (Pieruschka and Safran 1995)

$$g_{ff}(r) \approx g_{ff}^{(\infty)}(r) \equiv (S/V)^2 + \frac{2}{\pi^2}\left(\tau g(r)^2 - \frac{2}{3}g'(r)^2 + \frac{1}{9\tau}g''(r)^2\right) \tag{14}$$

where (Teubner 1991)

$$\tau \equiv \frac{\langle k^2\rangle}{3} = \left(\frac{\pi}{2}\right)^2\left(\frac{S}{V}\right)^2 \tag{15}$$

and $S/V$ is the amount of interface per unit volume, which is related to the membrane volume fraction by $\psi = \delta_0(S/V)$. Here, $g(r)$ is the bulk correlation function,

$$g(r) = \frac{a\xi}{8\pi}\exp(-r/\xi)\frac{\sin(kr)}{kr} \tag{16}$$

where

$$a = a_0\frac{k_BT}{\kappa}\frac{S}{V} \qquad \text{with } a_0 = \frac{15\pi^2}{16} \tag{17}$$

which is obtained by a Fourier transformation from the spectral density

$$\nu(q) = \frac{a}{q^4 - bq^2 + c}. \tag{18}$$

The characteristic wavenumber $k$ and the correlation length $\xi$ in (16) are given by (Teubner and Strey 1987)

$$k = (\sqrt{c/4} + b/4)^{1/2} \qquad \xi = (\sqrt{c/4} - b/4)^{-1/2}. \tag{19}$$

The coefficients $b$ and $c$ in (18) were calculated by Pieruschka and Safran (1993, 1995). For sufficiently large $\kappa$, these results reduce to

$$b = \frac{3}{2}\pi^2\left(\frac{S}{V}\right)^2 \qquad c = \left(\frac{3\pi^2}{4}\right)^2\left(\frac{S}{V}\right)^4. \tag{20}$$

For small $r$, on the other hand, Porod's law requires (Teubner 1990)

$$g_{ff}(r) = g_{ff}^{(0)}(r) \equiv \frac{S}{V}\frac{1}{2r}. \tag{21}$$

We combine these two asymptotic results by assuming that the short-range correlations given by (21) decay exponentially on a length scale which is proportional to the domain size, $d = 2\pi/k$, i.e. we approximate the full film correlation function by

$$g_{ff}(r) = g_{ff}^{(0)}(r)\exp(-kr) + g_{ff}^{(\infty)}(r). \tag{22}$$

The calculation of the Fourier transform of (14) and (22) can be performed without any further approximations. The result of this calculation is (Endo *et al* 2001)

$$S_{ff}^{(\infty)}(Q) = \frac{1}{8\pi^3}\frac{a^2\xi}{k^2}\left((\tau\xi^2)I_1(Q\xi,k\xi) - \frac{2}{3}I_2(Q\xi,k\xi) + \frac{1}{9\tau\xi^2}I_3(Q\xi,k\xi)\right) \tag{23}$$

where the explicit form of $I_1 \cdots I_3$ is too lengthy to be reproduced here, but can be found in the original publication. The full scattering function is then given by

$$S_{ff}(Q) = S_{ff}^{(\infty)}(Q) + 4\pi\frac{S}{2V}\frac{\xi^2}{(Q\xi)^2 + (k\xi)^2}. \tag{24}$$

The generic shape of $S_{ff}(Q)$ is a $1/Q$ behaviour for small $Q$ (but not too small, so that $Q\xi > 1$), followed by a peak or shoulder at $Q = 2k$, and a $1/Q^2$ decay for large $Q$. By construction, our result (24) reproduces the exact asymptotic scattering intensities for both small and large $Q$. The intensity in the vicinity of the peak or shoulder is, strictly speaking, beyond the validity of the approximation (24), but captures the main features of the scattering intensity calculated with the (numerically) exact expression for $g_{ff}(r)$ (Pieruschka and Safran 1995).

The approximation (24) has the advantage that it can easily be fitted to experimental data. Such fits can then be used to extract the value of the bending rigidity $\kappa$ (Endo *et al* 2001).

## 3. Phase behaviour

In this work, we consider microemulsions consisting of water, n-decane and non-ionic surfactant (alkyl polyglycolethers). To these ternary microemulsions we added amphiphilic block copolymers of the PEP$x$–PEO$y$ type, where $x$ and $y$ denote the molecular weights of each block in kg mol$^{-1}$. These block copolymers have similar structures as the $C_iE_j$ surfactants and differ from it mainly by their size and the methyl side groups of the hydrophobic PEP-block. The PEP–PEO block copolymers were synthesized by anionic polymerization. A detailed description of the polymer synthesis can be found in Allgaier *et al* (1997). The samples were prepared by weighing the components into test tubes. The tubes were sealed with polyethylene stoppers and the occurring phases were observed as a function of temperature. The observation of the phase diagrams was done in a thermostated water bath, where the temperature was controlled to within 0.02 K. The occurrence of different phases was determined by visual inspection in both transmitted and scattered light. Crossed polarizers were used in order to detect the presence of the lamellar phase.

### *3.1. The ternary system*

At equal volume fractions of water and oil, ternary microemulsions of water, n-alkane and $C_iE_j$ as a function of temperature display phase boundaries with a symmetric shape well known as 'fish'. In figure 1 such a fish is shown for the system $H_2O$–n-octane–$C_8E_3$ (open symbols), as presented by Strey *et al* (2001).

At low temperature an oil-in-water microemulsion coexists with an upper oil excess phase (denoted by $\underline{2}$), while at high temperature a water-in-oil phase coexists with a lower water excess phase (denoted by $\overline{2}$). At intermediate temperatures and low surfactant mass fractions

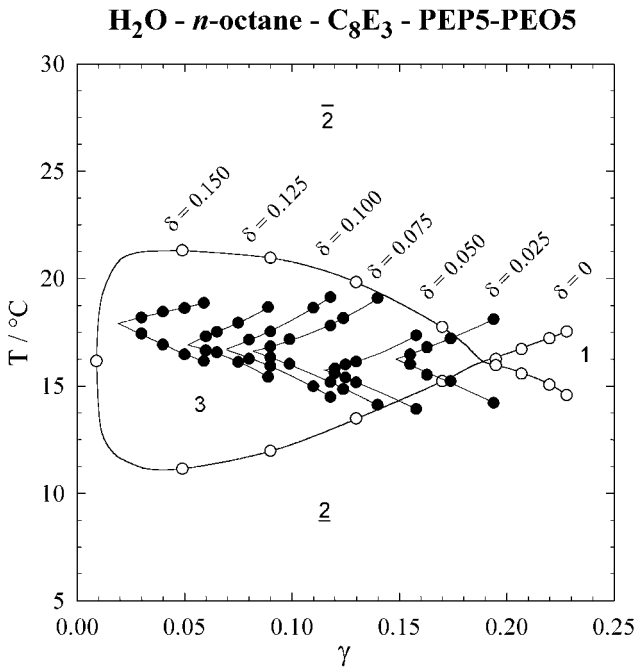


**Figure 1.** The section through the phase prism of water–n-octane–$C_8E_3$ at equal volumes of water and n-octane yields the well-known 'fish' (hollow circles). The effect of adding amphiphilic polymer (PEP5–PEO5) is an efficiency increase (full circles) at only slightly changed hydrophilic–lipophilic balance temperature.

$\gamma$, a three-phase body appears (upper oil excess phase, middle-phase microemulsion and lower water excess phase, denoted by 3). In the fish tail at intermediate temperatures and somewhat higher surfactant concentrations a one-phase region occurs (denoted by 1) which is the bicontinuous microemulsion. The fish-tail point where the one-phase region and the three-phase region meet is the landmark of the efficiency of a surfactant. It is denoted by its surfactant mass fraction $\tilde{\gamma}$ and temperature $\tilde{T}$. The lower $\tilde{\gamma}$ the more efficient a surfactant is said to be. The fish tail point at $\tilde{\gamma}$, $\tilde{T}$ is referred to as the X-point.

### *3.2. Efficiency boosting by the amphiphilic block copolymer*

The striking effect of adding the polymer PEP5–PEO5 on the X-point is demonstrated by the full circles in figure 1. These mark the fish-tail points for increasing polymer mass fraction $\delta$ in the surfactant/polymer mixture. The addition of polymer so that $\delta = 0.10$ leads to a reduction of $\tilde{\gamma}$ to $\tilde{\gamma} = 0.083$. Proceeding to $\delta = 0.15$ the minimum amount of surfactant plus polymer to form a one-phase microemulsion drops to $\tilde{\gamma} = 0.035$. Remarkably, the addition of PEP5–PEO5 does not lead to the formation of the lamellar phase in the fish tails presented in figure 1. Only in the most efficient fish tail, that is for $\delta = 0.15$, does the lamellar phase appear as an island at $\gamma > 0.1$. In all other cases only strong streaming birefringence is observed. In spite of the small quantities of polymer added a striking efficiency enhancement is achieved. It becomes increasingly difficult to extend the measurements to values of $\gamma < 0.02$, because of the extremely strong light scattering of the microemulsion phase. As mentioned above and as is evident from figure 1, the efficiency enhancement by polymer addition is obtained with

rather small shifts of the hydrophilic–lipophilic balance temperature. At closer inspection (cf table 1) for the larger $\delta$ a slight increase is visible due to the slightly more hydrophilic nature of PEP5–PEO5 compared to $C_8E_3$. This shift will be analyzed in section 3.5 and identified as a change in the spontaneous curvature $c_0$.

**Table 1.** Numerical values for the X-points of the water–n-octane–$C_8E_3$–PEP5–PEO5 system. The sample composition is given in terms of the mass fractions $\alpha = m_{oil}/(m_{oil} + m_{water})$, $\gamma = (m_{surfactant} + m_{polymer})/(m_{oil} + m_{water} + m_{surfactant} + m_{polymer})$ and $\delta = m_{polymer}/(m_{surfactant} + m_{polymer})$. The values of the dimensionless polymer grafting density $\sigma(R_o^2 + R_w^2)$ are calculated with a 2% bulk solubility of the surfactant in oil and water, where $R_o$ and $R_w$ denote the end-to-end distances of corresponding PEP and PEO homopolymers, respectively. The temperatures in brackets contain systematic errors and are therefore less reliable.

| $\alpha$ | $\tilde{\gamma}$ | $\delta$ | $\sigma(R_o^2 + R_w^2)$ | $\tilde{T}$ |
|---|---|---|---|---|
| 0.4130 | 0.1910 | 0.000 | 0.0 | 16.05 |
| 0.4130 | 0.1490 | 0.025 | 0.141 | 16.50 |
| 0.4130 | 0.1290 | 0.050 | 0.293 | (15.90) |
| 0.4130 | 0.0840 | 0.075 | 0.471 | 16.70 |
| 0.4130 | 0.0680 | 0.100 | 0.666 | 16.50 |
| 0.4130 | 0.0550 | 0.125 | 0.895 | 16.90 |
| 0.4130 | 0.0185 | 0.150 | 1.946 | (17.85) |

### *3.3. Effect of surfactant chain length*

Without added polymer, an increase of the hydrophilic head group size by one oxyethylene (O–$CH_2$–$CH_2$) unit, from $C_8E_3$ to $C_8E_4$, leads to a shift of the 'fish' to $\tilde{T} = 41.7\,^\circ$C, and to an increase of the surfactant mass fraction to $\tilde{\gamma} = 0.239$. Proceeding to $C_8E_5$, the fish is systematically shifted further upwards on the temperature scale, to $\tilde{T} = 61.5\,^\circ$C, and $\tilde{\gamma}$ increases to $\tilde{\gamma} = 0.283$. The X-points are given in figure 2 as open circles.

The same observation can be made for surfactants with larger hydrocarbon tails, i.e. a surfactant of larger hydrophobicity. Without added polymer, increasing the hydrophobic tail by two $CH_2$ groups, i.e. proceeding, for example, from $C_8E_5$ to $C_{10}E_5$ and to $C_{12}E_5$ at constant oxyethylene number, a significant efficiency increase is observed. The corresponding X-points are also included in figure 2. The mean temperature in general drops while $\tilde{\gamma}$ decreases. In numbers, for $C_{10}E_5$ we find $\tilde{T} = 44.6\,^\circ$C and $\tilde{\gamma} = 0.141$, and for $C_{12}E_5$ $\tilde{T} = 32.6\,^\circ$C and $\tilde{\gamma} = 0.048$. For $C_{14}E_5$ the efficiency increase leads to the collision of the lamellar mesophase with the three-phase body and the X-points cannot be determined.

With the addition of the amphiphilic block copolymer, a very similar efficiency boosting is observed for all surfactants (see the full points in figure 2). Note that we choose a logarithmic surfactant axis. In this representation it is clearly visible that the polymeric amphiphile causes the same relative efficiency boosting.

The lamellar mesophases usually increase in extent with increasing efficiency of the surfactant. In the experiments with added polymers we find that the lamellar phase is more destabilized—in comparison with equally efficient systems—for the shorter surfactant chain lengths. As an example, consider that a $C_{12}E_5$ microemulsion reaches $\gamma = 0.05$ with $\delta = 0$, displaying the lowest appearance of a lamellar phase in the form of a tip at $\gamma = 0.07$. A $C_{10}E_4$ microemulsion reaches $\gamma = 0.05$ with $\delta = 0.09$, displaying the lamellar tip at $\gamma = 0.12$. A $C_8E_3$ microemulsion reaches $\gamma = 0.05$ with $\delta = 0.11$, displaying no lamellar phase up to surfactant concentrations of $\gamma = 0.30$. The extent of the lamellar phase is the subject of ongoing research and will be published in due course.

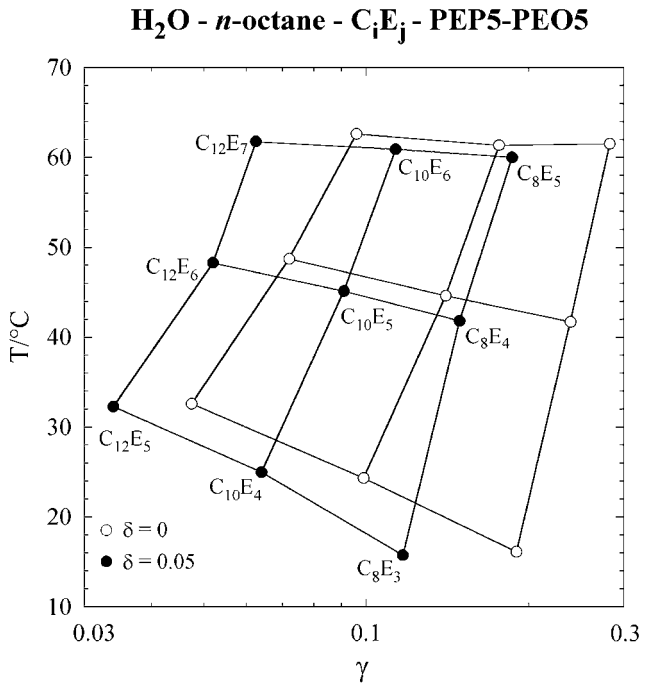


**Figure 2.** The characteristic X-points for water–n-octane–$C_iE_j$ systems (open circles) form a grid if both the surfactant tail chain length $i$ and the number of ethyleneoxide $j$ are varied. The similar magnitude of the boosting effect by adding $\delta = 0.05$ of amphiphilic block copolymer PEP5–PEO5 is demonstrated by the logarithmic $\gamma$-axis.

### *3.4. Contrast variation*

In order to perform SANS experiments under polymer contrast, the matching of oil, water and surfactant has to be achieved. For this purpose a fully deuterated $C_{10}E_4$ had to be synthesized. Details are given in Endo *et al* (2001). The samples for the structural investigations by SANS were prepared using $D_2O$, hydrogenous n-decane (h-decane) for the oil–water or bulk contrast and $D_2O$ and deuterated n-decane (d-decane) for the film contrast. We note that the phase diagrams for microemulsions prepared on the basis of $D_2O$ are shifted in temperature by about 2 K to lower values compared to those with $H_2O$. On the other hand, microemulsions containing d-$C_{10}E_4$, $D_2O$ and d-decane are shifted by about 7 K upwards compared to the microemulsions containing only hydrogenated materials. However, the X-points remain at the same surfactant concentration, independently of deuterated or hydrogenated material.

### *3.5. Comparison with theory*

The theoretical considerations of section 2.2 predict an exponential dependence of the membrane volume fraction $\psi$ on the dimensionless grafting density $\sigma(R_o^2 + R_w^2)$. Since the contribution of polymer anchoring points to the membrane area is extremely small in our systems, the membrane volume fraction $\psi$ can be identified with the surfactant volume fraction $\Phi_\gamma$. The data of the X-points in the systems water, n-decane, $C_{10}E_4$ and various PEP$x$–PEO$y$ block copolymers are shown in figure 3 in such a scaling plot. All data collapse onto a single straight line, which nicely confirms the scaling law (11). A fit to the data points

gives the slope

$$\Xi = 1.54 \pm 0.05. \tag{25}$$

which is roughly twice as large as the theoretical estimate (12). This indicates that the real, self-avoiding chains in our experiments have a considerably more pronounced effect on the curvature elastic moduli than ideal chains.

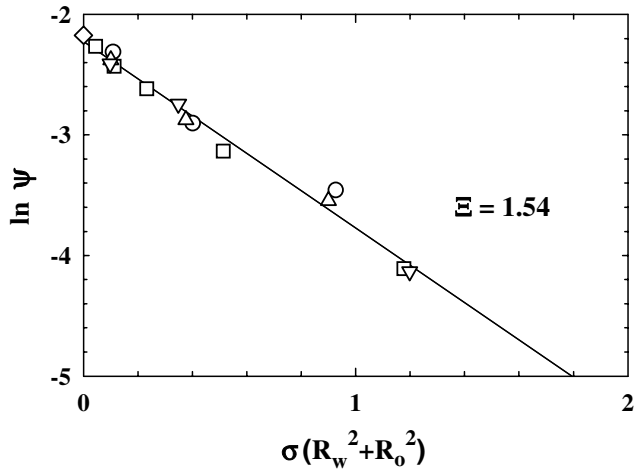


**Figure 3.** Membrane volume fraction $\psi$ of water–n-decane–$C_{10}E_4$–PEP$x$–PEO$y$ mixtures at the optimal point against scaled polymer grafting density $\sigma(R_w^2 + R_o^2)$. Pure system (◇), PEP5–PEO5 (▽), PEP10–PEO10 (△), PEP22–PEO22 (□), PEP5–PEO15 (○).

The temperatures of the X-points in figure 1 and table 1 are consistent with a linear dependence of $\tilde{T}$ on the dimensionless grafting density, with

$$\tilde{T} = \bar{T} + \mu_T \sigma (R_o^2 + R_w^2) \tag{26}$$

where $\bar{T} = 16.2\,^{\circ}$C and $\mu_T = 0.71 \pm 0.27$ K.

Experimentally, an almost linear temperature dependence of the mean curvature $\langle H \rangle$ of microemulsion droplets at coexistence has been found from the analysis of scattering data of ternary mixtures (Strey 1994, Sottmann and Strey 1997). For water, octane and $C_8E_3$, this relation is given by (Sottmann and Strey 1997)

$$\langle H \rangle = \mu_H (\bar{T} - T) \tag{27}$$

with $\mu_H = 1.9 \times 10^{-3}$ Å$^{-1}$ K$^{-1}$. On the other hand, in the curvature–elasticity model the mean curvature is found to be $\langle H \rangle = c_0(1 + \bar{\kappa}/2\kappa)^{-1}$ when thermal fluctuations are neglected. Under the assumption of $\bar{\kappa} \simeq -\kappa/2$, which is supported by experimental data (Sottmann and Strey 1997, Hellweg and Langevin 1998), this implies

$$c_0(\tilde{T}) = \Upsilon \sigma (R_o^2 + R_w^2) \tag{28}$$

with $\Upsilon = \Upsilon_1 \equiv \frac{3}{4}\mu_H \mu_T = (1.0 \pm 0.4) \times 10^{-3}$ Å$^{-1}$.

On the other hand, from the right-hand side of (10), we expect

$$\Upsilon = \frac{1}{4}\sqrt{\frac{\pi}{6}} \frac{k_B \tilde{T}}{\kappa_{eff}} \frac{R_w - R_o}{R_o^2 + R_w^2} \tag{29}$$

with $R_w = R_{PEO} = 77$ Å for PEO5 in water (Kawaguchi *et al* 1997), $R_o = R_{PEP} = 67$ Å for PEP5 in cyclohexane (Fetters, unpublished results), and $\kappa_{eff}/k_BT \simeq 0.7$ (Sottmann and Strey 1997), this implies $\Upsilon = \Upsilon_2 \equiv 0.25 \times 10^{-3}$ Å$^{-1}$.

Several explanations are conceivable for the discrepancy by about a factor four between the two values of $\Upsilon$. First, the scatter of the temperatures of the X-points is quite large, as can be seen from table 1. The error of the slope $\mu_T$, which we obtain from a linear regression analysis, may therefore be underestimated. Second, the calculation of the spontaneous curvatures from the measured mean curvatures neglects the translational entropy of the droplets. Third, the value of $\Upsilon$ in (29) depends very sensitively on the *difference* of the end-to-end distances of the two blocks, both of which have been measured only indirectly (for a detailed discussions of the measurement of the end-to-end distances see Endo *et al* (2001)). Finally, the theoretical expression (29) is based on a calculation for ideal chains. It is quite possible that the universal prefactor in this relation is larger for real, self-avoiding chains.

It is clear that a more stringent comparison of theory and experiment on the spontaneous-curvature effect of amphiphilic block copolymers requires a compilation of data for systems with an increasing asymmetry of the two polymer blocks. Such an investigation is in progress.

## 4. Neutron scattering and structure

In order to understand the mechanism behind the efficiency boosting by amphiphilic polymers it is of great importance to investigate the role of these polymers in the four-component microemulsion on a mesoscopic scale. SANS together with contrast variation by hydrogen–deuterium exchange are the methods of choice for this undertaking.

### *4.1. Partial structure factors*

The small-angle scattering of neutrons arises from fluctuations of the scattering length densities $\rho_i = (\sum_j b_j)/v_i$ where $b_j$ are the scattering lengths of different atoms in a molecule $i$ and $v_i$ is the volume of the corresponding molecule. Under the assumption of incompressibility and with the definition of one of the molecular species as reference—its scattering length density may be denoted by $\rho_s$—the coherent scattering cross section per volume is given by

$$I(Q) = \sum_{i,j} (\rho_i - \rho_s)(\rho_j - \rho_s) S_{ij}(Q) \tag{30}$$

with the partial structure factors (see, e.g., Bacon (1975))

$$S_{ij}(Q) = \frac{1}{V} \int_V \langle \phi_i(\boldsymbol{r}) \phi_j(\boldsymbol{r}') \rangle \exp[\mathrm{i}\boldsymbol{Q} \cdot (\boldsymbol{r} - \boldsymbol{r}')] \, \mathrm{d}^3 r \, \mathrm{d}^3 r'. \tag{31}$$

The integration is performed over the sample volume and $\phi_i(\boldsymbol{r})$ describes the volume fraction of molecule $i$ at a position $\boldsymbol{r}$. $|\boldsymbol{Q}| = (4\pi/\lambda)\sin(\Theta/2)$ is the scattering wavenumber with $\Theta$ the scattering angle and $\lambda$ the neutron wavelength. For a quaternary microemulsion containing oil, water, surfactant and polymer, the scattering intensity may be described in terms of partial structure factors

$$\begin{aligned} I(Q) = {} & (\rho_o - \rho_w)^2 S_{oo}(Q) + (\rho_f - \rho_w)^2 S_{ff}(Q) + (\rho_p - \rho_w)^2 S_{pp}(Q) \\ & + 2(\rho_o - \rho_w)(\rho_f - \rho_w) S_{of}(Q) + 2(\rho_f - \rho_w)(\rho_p - \rho_w) S_{fp}(Q) \\ & + 2(\rho_o - \rho_w)(\rho_p - \rho_w) S_{op}(Q) \end{aligned} \tag{32}$$

where $o$, $w$, $f$ and $p$ indicate oil, water, film and polymer, respectively. Water has here been used as the reference indicated above. Considering the very low polymer volume fraction in the microemulsion, in general we may neglect the partial scattering functions $S_{pp}$, $S_{fp}$ and $S_{op}$, which are buried under the $S_{oo}$ and $S_{ff}$ contributions in (30). For $\rho_f = \rho_w$, the scattering intensity $I(Q)$ then reveals $S_{oo}(Q)$, which we call 'bulk contrast'. On the other

hand, for $\rho_o = \rho_w$; $I(Q) = (\rho_f - \rho_w)^2 S_{ff}(Q)$. For this 'film contrast' the experiment reveals information about the surfactant correlations.

If $\rho_w$, $\rho_o$ and $\rho_f$ are precisely matched, then the scattering intensity will be dominated by $S_{pp}(Q)$, and we may obtain information about the structure of the polymer. This contrast is called 'polymer contrast'. We further note that the off-diagonal partial structure factors $S_{of}$, $S_{op}$ and $S_{fp}$ also contain valuable information; $S_{fp}$, in particular, reveals the density profile of the polymers tethered to the surface.

### *4.2. Polymer–film and polymer–polymer partial structure factors*

Let us assume that the amphiphilic polymer is tethered to the surfactant layer with the hydrophilic PEO part in the water and the hydrophobic PEP part in the oil phase.

For ideal chains, the monomer density, $\phi_p(z)$, of polymers anchored to a planar wall located at $z = 0$ constitutes the so-called mushroom regime with a polymer density profile (Eisenriegler *et al* 1982)

$$\phi_p(z) = \frac{\sqrt{6\pi}}{R_e}\left[\operatorname{erfc}\left(\frac{1}{2}\sqrt{6}\frac{z}{R_e}\right) - \operatorname{erfc}\left(\sqrt{6}\frac{z}{R_e}\right)\right] \tag{33}$$

as a function of the distance $z$ from the wall, where $R_e$ is the end-to-end distance of a free polymer chain, and $\operatorname{erfc}(x)$ is the complement of the error function. The real end-to-end distance of an anchored polymer is of course larger than $R_e$. For ideal chains, the average end-to-end distance *parallel* to the wall is the same as in the bulk solution, whereas the anchored polymers are more extended by a factor of $\sqrt{2}$ *perpendicular* to the wall. The amplitude in (33) is defined by the normalization $\int_0^\infty \phi_p(z)\,\mathrm{d}z = 1$. The monomer density vanishes at the wall, has a maximum at $z/R_e = 4\ln 2/(3\sqrt{6}) = 0.377$ and decays exponentially for $z \gg R_e$.

The polymer scattering amplitude is obtained from the one-dimensional Fourier transform of the symmetrized density profile. Due to the simple analytical form of $\phi_p(z)$, this can also be calculated exactly. Thereby we find

$$P(QR_e) = \frac{2\sqrt{6}}{QR_e}\left[D\left(\frac{QR_e}{\sqrt{6}}\right) - D\left(\frac{QR_e}{2\sqrt{6}}\right)\right] \tag{34}$$

where $D(x)$ is Dawson's integral.

The partial structure factor $S_{fp}(Q)$, the interference term between polymer and film scattering, follows from the product of the corresponding scattering amplitudes. For an asymmetric PEP–PEO block copolymer with a relative PEP volume fraction $f$ the normalized scattering amplitude from the polymer density is obtained by the (symmetrized) Fourier transformation $P(QR_e)$ of the monomer-density profile, given in (34),

$$A_p^z(Q) = fP(QR_o) + (1-f)P(QR_w). \tag{35}$$

For a locally flat film of thickness $t$, the corresponding amplitude is $A_f = \sin(Qt/2)/(Qt/2)$. In order to arrive at $S_{fp}(Q)$, the product $A_f(Q)A_p(Q)$ has to be orientationally averaged over all surface directions within the microemulsion, which leads to a $1/Q^2$ factor in the high-$Q$ regime.

In this asymptotic $Q$-regime, but at not too large $Q$ so that $A_f \simeq 1$, $S_{fp}(Q)$ mirrors directly the (symmetrized) perpendicular polymer density profile

$$S_{fp}(Q) \simeq \frac{1}{Q^2}A_p^z(Q). \tag{36}$$

The polymer–polymer partial structure $S_{pp}$ from the tethered polymers may be separated into two parts: (i) the scattering from the average density profile $\phi_p(z)$; and (ii) the diffuse

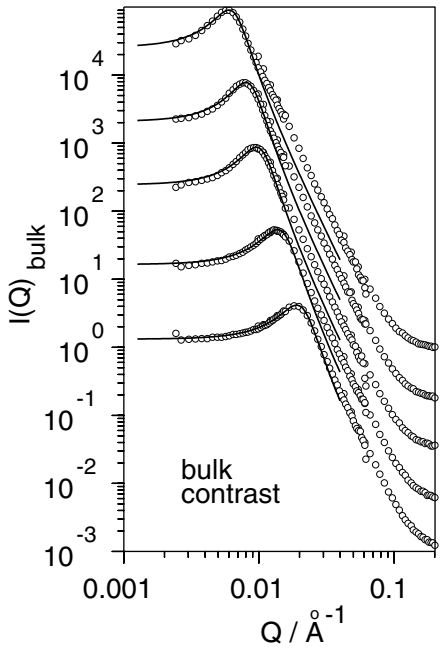


**Figure 4.** Bulk-contrast SANS data from bicontinuous microemulsion phases close to the fish-tail point in the system water–n-decane–$C_{10}E_4$–PEP10–PEO10. The curves correspond to different relative polymer content in the surfactant $\Phi_\delta = V_{polymer}/(V_{surfactant} + V_{polymer})$ and as a consequence different decreasing total surfactant content $\Phi_\gamma = (V_{surfactant} + V_{polymer})/(V_{water} + V_{oil} + V_{surfactant} + V_{polymer})$. The values are $(\Phi_\gamma, \Phi_\delta) = (0.045, 0.101)$; $(0.060, 0.070)$; $(0.072, 0.048)$, $(0.100, 0.023)$ and $(0.133, 0.000)$. The curves are separated from each other by a shift factor of five, the intensity scale applies directly to the uppermost curve. The symbols indicate the data, the full curves the fit with equation (18).

scattering from the correlations of monomers within the chain and possibly among different chains in the lateral direction. For infinite planar surfaces, this would be all. For a bicontinuous phase with locally varying curvature, we have to consider further the correlations of the polymers mediated by the tethering to the surfactant film.

The polymer–polymer partial structure factor $S_{pp}(Q)$, which arises from the polymer-decorated surfactant layer, may be written as

$$S_{pp}(Q) = \mathcal{N} S_{ff}(Q)\{A_p^z(Q)\}^2 + \tilde{S}_{pp}(Q). \tag{37}$$

The first term describes the scattering from the surfactant film $S_{ff}(Q)$ with a normalization factor $\mathcal{N}$ related to the decoration density (see Endo *et al* (2001)).

The polymer density profile gives rise to a form factor $\{A_p^z(Q)\}^2$, which is the square of the respective scattering amplitude. $\tilde{S}_{pp}(Q)$ results from the monomer-density fluctuations discussed above.

### *4.3. Double contrast variation*

Polymer scattering may be observed, if the scattering length densities of water, oil and surfactant are precisely matched. Then in principle a single protonated chain in the deuterated environment will give rise to the signal from the individual polymer chains. However, since in

microemulsion systems the very large intensity differences between the scattering under bulk (order of magnitude $10^5$ cm$^{-1}$), film ($10^2$ cm$^{-1}$) and polymer contrast (below 1 cm$^{-1}$) need to be accounted for, in practice such an approach does not work.

The problem becomes treatable by employing a two-dimensional contrast variation scheme around the total matching point of oil, water and surfactant. With a sufficient over-determination of (32)—in the case of the polymers in the microemulsion 15 different contrasts were measured—equation (32) may be solved for $S_{ij}(Q)$ by using a singular value decomposition scheme (Endo *et al* 2001) which is equivalent to a least-squares fit. For that purpose all scattering length densities have to be precisely known—a task which is carried out by supporting NMR and density measurements.

In order to improve further the stability and correctness of the solutions, $S_{oo}(Q)$ and $S_{ff}(Q)$ which are known from respective film and bulk contrast measurements, may be introduced. Furthermore, the relation $S_{af}(Q) = -1/2$, $S_{ff}(Q)$ can be employed (Endo *et al* 2001). This data evaluation leads to the partial structure factors $S_{pp}$, $S_{fp}$ and $S_{op}$. While the results for $S_{pp}$ and $S_{fp}$ are stable with respect to small variations of the matching point between oil and water, $S_{op}$ is strongly affected and therefore cannot be determined reliably.

### *4.4. Experimental partial structure factors*

In this section we present SANS results on four different partial structure factors $S_{oo}$, $S_{ff}$, $S_{fp}$ and finally $S_{pp}$. The first two structure factors are interpreted theoretically in terms of predictions by the Gaussian random field theory as elaborated in section 2.3. $S_{fp}$ and $S_{pp}$ are discussed in terms of the concept outlined in the preceding paragraph.

*4.4.1. The bulk structure factor $S_{oo}$.* SANS data under bulk contrast have been taken on five different samples of symmetric $D_2O$/h-decane mixtures containing different amounts of surfactant and polymer such that the fish-tail point was always realized. Figure 4 displays the synopsis of the SANS data. All the structure factors are characterized by a plateau at low $Q$, a peak at intermediate $Q$ and a $Q^{-4}$ high-$Q$ flank. With decreasing overall surfactant volume fraction $\Phi_\gamma = (V_{surfactant} + V_{polymer})/(V_{water} + V_{oil} + V_{surfactant} + V_{polymer})$—made accessible by increasing the polymer concentration $\Phi_\delta = V_{polymer}/(V_{surfactant} + V_{polymer})$—the scattering curves are displaced to lower $Q$ and at the same time gain intensity. Furthermore, the peak appears to sharpen. The data immediately reveal an increasing domain size $d \simeq 2\pi/Q_{max}$ with increasing polymer volume fraction. The SANS data were fitted with (18) extracting thereby both the domain size $d$ as well as the correlation length $\xi$. The results are listed in table 2.

**Table 2.** Characteristic length scales, domain size $d = 2\pi/k$ and correlation length $\xi$, cf (19), from a fit of the bulk-contrast data to (18). The sample composition is given in terms of the volume fractions $\Phi_\alpha = V_{oil}/(V_{water} + V_{oil})$, $\Phi_\gamma = (V_{surfactant} + V_{polymer})/(V_{water} + V_{oil} + V_{surfactant} + V_{polymer})$, and $\Phi_\delta = V_{polymer}/(V_{surfactant} + V_{polymer})$.

| $\Phi_\alpha$ | $\Phi_\gamma$ | $\Phi_\delta$ | $d$ (Å) | $\xi$ (Å) |
|---|---|---|---|---|
| 0.51 | 0.131 | 0.000 | 314 | 162 |
| 0.50 | 0.100 | 0.022 | 436 | 229 |
| 0.50 | 0.077 | 0.048 | 629 | 350 |
| 0.50 | 0.063 | 0.070 | 755 | 432 |
| 0.50 | 0.049 | 0.102 | 1003 | 553 |

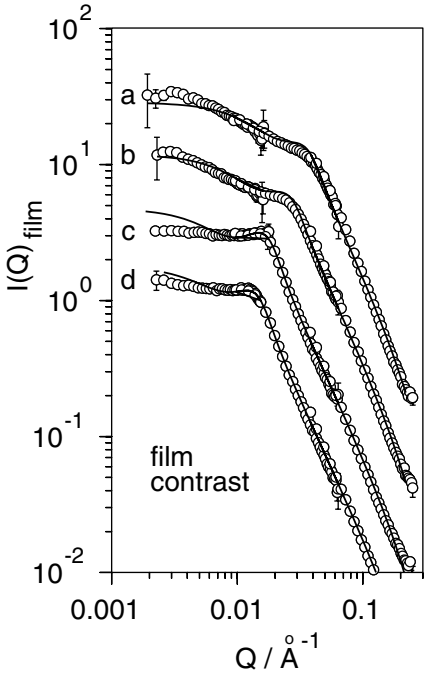


**Figure 5.** Film-contrast SANS data from bicontinuous microemulsion phases close to the fish-tail point in the system water–n-decane–$C_{10}E_4$–PEP10–PEO10. Open symbols are the experimental points, with (a) $\Phi_\delta = 0$, (b) $\Phi_\delta = 0.032$, (c) $\Phi_\delta = 0.083$ and (d) $\Phi_\delta = 0.110$. The intensity scale applies directly to (a), while (b) and (c) are successively shifted by a factor of 0.3. Full curves correspond to fits with the Gaussian random field expression, equation (24) (see Endo *et al* (2001) for details).

*4.4.2. The film structure factor $S_{ff}$.* The relation between the film and bulk scattering reveals itself from studies under film contrast on samples with compositions as close as possible to the bulk contrast samples discussed above.

Since all microemulsions were studied close to the fish-tail point, increasing the polymer volume fraction leads to a reduction of the overall surfactant volume fraction $\Phi_\gamma$ because the fish tail is shifting. Figure 5 displays the experimental results obtained for different polymer surfactant compositions. The data traces are composed of a low-$Q$ plateau, which crosses over to a high-$Q$ asymptotic $1/Q^2$ behaviour. With increasing polymer concentration, the knee which is the crossover from the low to the high-$Q$ regime shifts towards lower $Q$ in accordance with what is seen for the bulk data. The full curves in figure 5 display a fit with the predictions, equation (24), of the random interface model. Thereby, the structural lengths $d$ and $\xi$ which were obtained from the bulk contrast samples were kept fixed. The bending rigidity $\kappa_{eff}$ may be calculated from the value of $a$ (equation (17)).

The bending rigidity we extract from the scattering data is affected by thermal membrane fluctuations on scales smaller than the average domain size—the value $a$ in (17) results mainly from this regime of length scales. Following the reasoning in section 2 it therefore constitutes $\kappa_R$, the renormalized bending elasticity (figure 6). It shows a rather weak dependence on the polymer grafting density, with a tendency to decreasing values with increasing polymer density. Inverting (7) we may derive the bare effective bending elasticity $\kappa_{eff}$ which is also shown in figure 6. It can be seen that $\kappa_{eff}(\sigma)$ is a linear function of $\sigma(R_w^2 + R_o^2)$, consistent

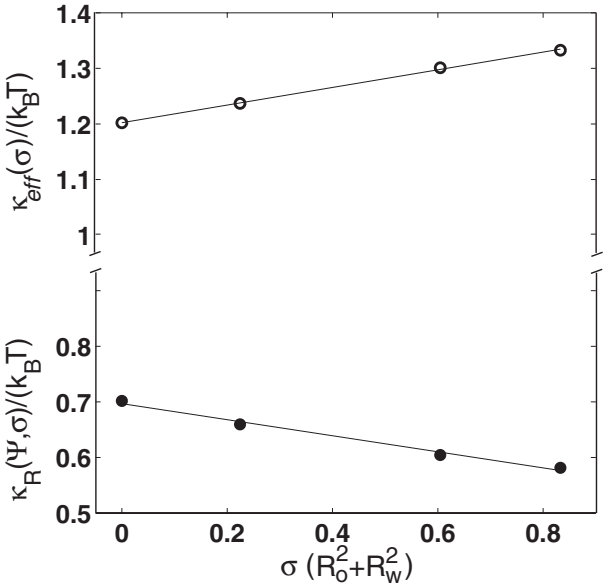


**Figure 6.** The estimated bending moduli $\kappa_R(\psi, \sigma)$ (lower half) and $\kappa_{eff}(\sigma)$ (upper half), determined from the fits of the data in figure 5 to equations (3) and (7). The system is the same as in figure 5.

with the prediction. Furthermore, a slope of 0.16 is found, which compares quite well with the theoretical value of $(1 + \pi/2)/12 = 0.214$, which is strictly valid only for ideal chains.

A detailed analysis of the film scattering intensities based on the expressions derived for Ginzburg–Landau models is given by Endo *et al* (2001).

*4.4.3. The polymer structure factor $S_{fp}$ and $S_{pp}$.* The partial scattering functions $S_{fp}(Q)$ and $S_{pp}(Q)$ contain information about the polymer. $S_{fp}(Q)$ is, in particular, sensitive to the projection of the average polymer density on the (local) normal direction to the interface. Any fluctuating segment–film correlations average to zero (Auroy *et al* 1990, Auroy and Auvray 1993, Auvray and de Gennes 1986). Whereas the latter statement stays valid for the curved interface of the bicontinuous structure, the projection property is only valid in the high-$Q$ limit where the membrane may be considered as flat. There a comparison with the theoretical considerations of section 4.2 can be made and the predictions for the polymer-density profile can be checked.

The $S_{fp}(Q)$ data and fits to (36) are shown in figure 7. The lines display (36) computed with $R_{PEO} = 161$ Å and $R_{PEP} = 80.5$ Å. For the fit procedure, the ratio $R_{PEP}/R_{PEO}$ was kept fixed. The fact that the data quickly approach zero at the high-$Q$ end corroborates the expectation that segment-film correlations are not seen in this partial scattering function.

These values should be compared with the end-to-end distances of the corresponding homopolymers in solutions, which have been found to be $R_{PEP} = 67$ Å for PEP5 in cyclohexane (Fetters, unpublished results) and $R_{PEO} = 138$ Å for PEO15 in water (Kawaguchi *et al* 1997). Since an error estimate of about 10% is not unreasonable in both types of measurements, we can conclude that the polymer coils behave as isolated, self-avoiding chains, which are neither attracted to the membrane nor compressed by other polymers.

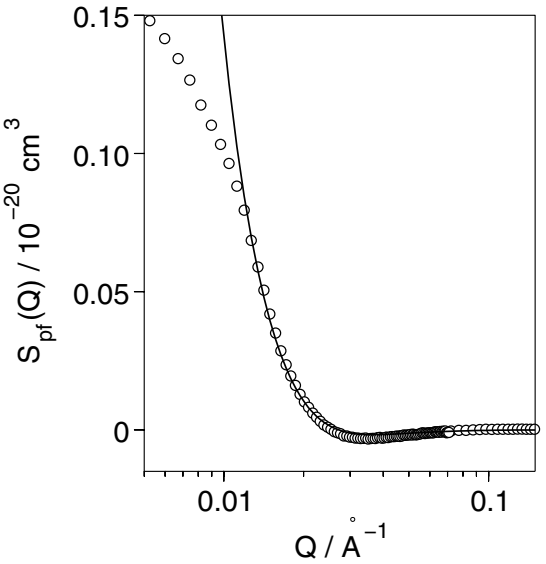


**Figure 7.** Partial scattering function $S_{fp}(Q)$ (circles) in the system water, n-decane, $C_{10}E_4$ and PEP5–PEO15. The curve corresponds to a fit to (36), which yields $R_{PEO} = 161$ Å and $R_{PEP} = 80.5$ Å. Since equation (36) is only valid in the high-$Q$ region, fits were performed to data in the $Q$-range $0.012 \leqslant Q/\text{Å}^{-1} \leqslant 0.2$.

The polymer–polymer scattering function contains both contributions due to the average polymer density and contributions due to fluctuating segmental correlations. The average density decorates the interface and is expected to be proportional to the film–film scattering multiplied by a polymer form factor as expressed in the first term of (37). Figure 8 shows $S_{pp}(Q)$ with fits to (37), the values of the end-to-end radii correspond to those obtained from the fit to $S_{fp}(Q)$ (figure 7). The polymer fluctuation contribution $\tilde{S}_{pp}(Q)$ is modelled by the fluctuation part of a Beaucage function (Beaucage 1996)

$$\tilde{S}_{pp}(Q) \propto (\text{erf}[w(QR_g)/\sqrt{6}]^3/(QR_g))^{\nu} \tag{38}$$

with a $Q^{-\nu}$ asymptote (with $\nu \simeq 5/3$), crossover length $\sqrt{6}R_g$ equal to the end-to-end radii and $w = 1.06$.

The deviations (missing intensity) at intermediate $Q$ most probably results from the neglect of lateral density fluctuations that result from the average density variation from the centre to the periphery of a polymer mushroom if projected onto the oil–water interface. The arrangement of mushrooms tethered to the interface resembles a two-dimensional soft-sphere fluid, the lateral correlation due to its structure factor would at least account for a fraction of the missing intensity. In addition, the used ansatz leading to the first term of (37) assumes flat interfaces, which is only valid in the limit of small curvatures.

## 5. Summary and conclusions

The detailed measurements of the efficiency boosting by amphiphilic block copolymers in the $C_{10}E_4$ system by Jakobs *et al* (1999) and in the $C_8E_3$ system described in this review are further supported by a study of the effect for a variety of other $C_iE_j$ systems. Interestingly, the boosting effect is quantitatively the larger the weaker the ternary base system. Jakobs *et al*

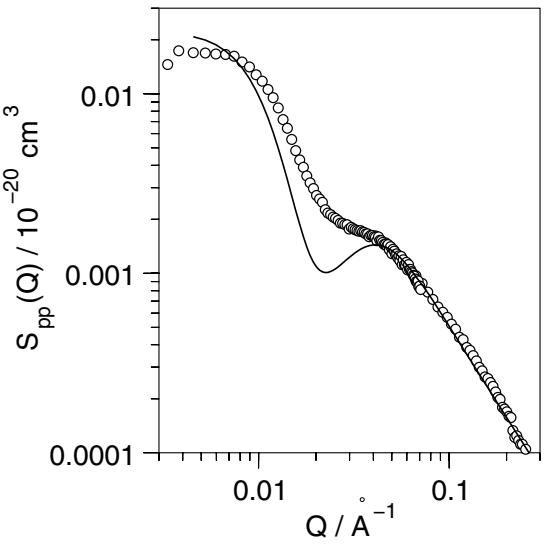


**Figure 8.** Partial scattering function $S_{pp}(Q)$ in the system water, n-decane, $C_{10}E_4$ and PEP5–PEO15. The curve corresponds to a fit with (37), the assumed end-to-end radii correspond to the values obtained from the fit shown in figure 7. The polymer fluctuation contribution $\tilde{S}_{pp}(Q)$ is modelled by a Beaucage function (38) with a $Q^{-\nu}$ asymptote ($\nu = 1.66$) and crossover lengths equal to the end-to-end radii.

(1999) reported the efficiency boosting effect to be observed for a variety of block copolymers of various block sizes. Also, it appears that the shorter the chain length of the surfactant of the base system, the more the lamellar phase is suppressed. All these observations led us to ask a number of questions which were solved by a series of SANS experiments and led to the adaptation of a theoretical approach based on the curvature elasticity of the polymer-decorated membrane (Endo *et al* 2000, 2001).

Adding block copolymers PEP$x$–PEO$y$ to a ternary base system results in an enormous efficiency increase, irrespective of the different surfactant and oil chain lengths or the size of the polymer blocks. The origin of this effect is apparently related to the ability of the block copolymer to extend into the adjacent sub-phases. SANS measurements in bulk and film contrast in addition to a double-contrast variation technique allow it to be stated clearly that effectively all the amphiphilic block copolymer molecules are embedded in the monolayer and decorate the amphiphilic film. In this fashion the individual block can extend into the preferred solvent, PEO into the water and PEP into the oil. Jakobs *et al* (1999) have reported that the efficiency boosting effect is accompanied by a comparatively large length scale increase in the microemulsion. Also a decrease of the ultra-low interfacial tension between water- and oil-rich phases was seen. Embedding the block copolymer into the amphiphilic film has a profound effect on the curvature and rigidity of monolayers and bilayers.

Recent theoretical calculations by Hiergeist and Lipowsky (1996) and Eisenriegler *et al* (1996), which describe the effects of anchored polymers on membrane elasticity, provide the basis of our theoretical discussion. In these papers, mushroom-like conformations of the individual blocks of anchored polymers on one side of the membrane or film are discussed. However, in our system we have to consider polymeric ends on both sides of the monolayer which oppositely affect curvature and jointly add to the bending elastic properties.

In fact, the effect of the polymer on the membrane elasticity is rather weak, and reaches only a fraction of $k_BT$ at the overlap concentration. It is therefore very difficult to observe for lipid bilayer membranes, which have typical bending rigidities of $10k_BT$ or more. This effect becomes dominant in ternary microemulsions, because it is amplified by the exponential dependence of the surfactant volume fraction on the elastic moduli of the membrane.

Furthermore, the addition of amphiphilic block copolymers provides the unique possibility of varying the elastic moduli of membranes in a controlled and systematic way. Therefore, this is an ideal system for a detailed comparison of theoretical models of microemulsions with experimental results.

In almost perfect agreement with most the recent theoretical developments (Morse 1994, Gompper and Kroll 1998), the efficiency increase is found to be associated with an increase in the saddle-splay modulus $\bar{\kappa}$. Increasing the bending rigidity $\kappa$, on the other hand, has the effect of stabilizing the lamellar phase in these systems. Therefore, if we start with a weaker, i.e. shorter chain surfactant, an efficiency boosting may be accomplished while at the same time stabilizing the lamellar phase less. The details of the last point are presently being examined in our laboratories and will be published in due course.

## Acknowledgments

We thank H Endo, B Jakobs, M Mihailescu, M Monkenbusch and T Sottmann for a very enjoyable collaboration and many stimulating discussions on this subject.

## References

Allgaier J, Poppe A, Willner L and Richter D 1997 *Macromolecules* **30** 1582
Andelman D, Cates M E, Roux D and Safran S A 1987 *J. Chem. Phys.* **87** 7229
Auroy P and Auvray L 1993 *J. Physique. II* **3** 227
Auroy P, Auvary L and Leger L 1990 *J. Phys.: Condens. Matter* **2** 317
Auvray L and de Gennes P G 1986 *Europhys. Lett.* **2** 647
Bacon G E 1975 *Neutron Diffraction* (Oxford: Clarendon)
Beaucage G 1996 *J. Appl. Crystalogr.* **29** 134
Berk N F 1987 *Phys. Rev. Lett.* **58** 2718
——1991 *Phys. Rev.* A **44** 5069
Cai W, Lubensky T C, Nelson P and Powers T 1994 *J. Physique* II **4** 931
Canham P B 1970 *J. Theor. Biol.* **26** 61
Cates M E, Roux D, Andelman D, Milner S T and Safran S A 1988 *Europhys. Lett.* **5** 733
Daicic J, Olsson U and Wennerström H 1995a *Langmuir* **11** 2451
Daicic J, Olsson U, Wennerström H, Jerke G and Schurtenberger P 1995b *Phys. Rev.* E **52** 3266
——1995c *J. Physique II* **5** 199
David F 1989 *Phys. Rep.* **184** 221
Eisenriegler E, Hanke A and Dietrich S 1996 *Phys. Rev.* E **54** 1134
Eisenriegler E, Kremer K and Binder K 1982 *J. Chem. Phys.* **77** 6296
Endo H, Allgaier J, Gompper G, Jakobs B, Monkenbusch M, Richter D, Sottmann T and Strey R 2000 *Phys. Rev. Lett.* **85** 102
Endo H, Mihailescu M, Monkenbusch M, Allgaier J, Gompper G, Richter D, Jakobs B, Sottmann T, Strey R and Grillo I 2001 *J. Chem. Phys.* **115** 5801
Golubović L 1994 *Phys. Rev.* E **50** R2419
Golubović L and Lubensky T C 1989 *Europhys. Lett.* **10** 513
——1990 *Phys. Rev.* A **41** 4343
Gompper G and Kroll D M 1996 *J. Physique I* **6** 1305
——1998 *Phys. Rev. Lett.* **81** 2284
——2000 *J. Phys.: Condens. Matter* **12** 29
Gompper G and Schick M 1994a *Phys. Rev.* E **49** 1478

Gompper G and Schick M 1994b *Phase Transitions and Critical Phenomena* vol 16, ed C Domb and J Lebowitz (London: Academic) pp 1–176
Helfrich W 1973 *Z Naturfosch.* **28c** 693
——1985 *J. Physique* **46** 1263
——1998 *Eur. Phys. J.* B **1** 481
Hellweg T and Langevin D 1998 *Phys. Rev.* E **57** 6825
Hiergeist C and Lipowsky R 1996 *J. Physique II* **6** 1465
Jakobs B, Scottmann T, Strey R, Allgaier J, Willner L and Richter D 1999 *Langmuir* **15** 6707
Kawaguchi S, Imai G, Suzuki J, Miyahara A, Kitano T and Ito K 1997 *Polymer* **38** 2885
Marques C M and Fournier J 1996 *Europhys. Lett.* **35** 361
Morse D C 1994 *Phys. Rev.* E **50** R2423
——1997 *Curr. Opin. Coll. Interface Sci.* **2** 365
Peliti L and Leibler S 1985 *Phys. Rev. Lett.* **54** 1690
Pieruschka P and Marčelja S 1992 *J. Physique II* **2** 235
——1994 *Langmuir* **10** 345
Pieruschka P and Safran S A 1993 *Europhys. Lett.* **22** 625
——1995 *Europhys. Lett.* **31** 207
Porte G 1992 *J. Phys.: Condens. Matter* **4** 8649
Porte G, Appell J, Bassereau P and Marignan J 1989 *J. Physique* **50** 1335
Porte G, Appell J and Marignan J 1997 *Phys. Rev.* E **56** 1276
Porte G, Delsanti M, Billard I, Skouri M, Appell J, Marignan J and Debeauvais F 1991 *J. Physique II* **1** 1101
Roux D, Cates M E, Olsson U, Ball R C, Nallet F and Bellocq A M 1990 *Europhys. Lett.* **11** 229
Roux D, Coulon C and Cates M E 1992 *J. Phys. Chem.* **96** 4174
Safran S A 1992 *Structure and Dynamics of Supramolecular Aggregates* ed S H Chen, J S Huang and P Tartaglia (Dordrecht: Kluwer)
Safran S A, Roux D, Cates M E and Andelman D 1986 *Phys. Rev. Lett.* **57** 491
Sottmann T and Strey R 1997 *J. Chem. Phys.* **106** 8606
Strey R 1994 *Colloid Polym. Sci.* **272** 1005
Strey R, Brandt M, Jakobs B and Sottmann T 2001 *Studies in Surface Science and Catalysis* ed Y Iwasawa, N Oyama and H Kunieda (Amsterdam: Elsevier) p 39
Teubner M 1990 *J. Chem. Phys.* **92** 4501
——1991 *Europhys. Lett.* **14** 403
Teubner M and Strey R 1987 *J. Chem. Phys.* **87** 3195
Tlusty T, Safran S A, Menes R and Strey R 1997 *Phys. Rev. Lett.* **78** 2616
Tlusty T, Safran S A and Strey R 2000 *Phys. Rev. Lett.* **84** 1244
Wennerström H and Olsson U 1993 *Langmuir* **9** 365